PERGAMON

Applied Radiation and Isotopes 50 (1999) 73–87

Applied Radiation and Isotopes

Radiation dosimetry in nuclear medicine

M.G. Stabin[a,*], M. Tagesson[b], S.R. Thomas[c], M. Ljungberg[b], S.E. Strand[b]

[a]*Radiation Internal Dose Information Center, Oak Ridge Associated Universities, P.O. Box 117, Oak Ridge, TN 37831-0117, U.S.A.*
[b]*Lund University Hospital, Department of Radiation Physics, 221 85 Lund, Sweden*
[c]*Division of Medical Physics, Medical Sciences Building, University of Cincinnati, E-560, Cincinnati, OH 45267-0579, U.S.A.*

Abstract

Radionuclides are used in nuclear medicine in a variety of diagnostic and therapeutic procedures. A knowledge of the radiation dose received by different organs in the body is essential to an evaluation of the risks and benefits of any procedure. In this paper, current methods for internal dosimetry are reviewed, as they are applied in nuclear medicine. Particularly, the Medical Internal Radiation Dose (MIRD) system for dosimetry is explained, and many of its published resources discussed. Available models representing individuals of different age and gender, including those representing the pregnant woman are described; current trends in establishing models for individual patients are also evaluated. The proper design of kinetic studies for establishing radiation doses for radiopharmaceuticals is discussed. An overview of how to use information obtained in a dosimetry study, including that of the effective dose equivalent (ICRP 30) and effective dose (ICRP 60), is given. Current trends and issues in internal dosimetry, including the calculation of patient-specific doses and in the use of small scale and microdosimetry techniques, are also reviewed.

1. Introduction

Radionuclides are administered to patients in nuclear medicine procedures in a variety of diagnostic and therapeutic applications. A key consideration in such studies is the absorbed dose to different organs of the patient; this concern is naturally heightened in therapy applications, where a significant absorbed dose may be received by other organs and in particular by radiosensitive organs. The purpose of this chapter is to review the methods and models used in internal dosimetry in nuclear medicine and discuss some current trends and challenges in this field. It is not our intention to catalog radiation dose for many nuclear medicine procedures; such dose estimate compendia may be found in various references (e.g. ICRP, 1988; Stabin *et al.*, 1996).

* To whom all correspondence should be addressed.

2. Internal dosimetry methods

2.1. Basic concepts

A generic equation for the absorbed dose in an organ is:

$$D = \frac{k\tilde{A}\sum_i n_i E_i \phi_i}{m} \quad (1)$$

where D = absorbed dose (rad or Gy); $\tilde{A}$ = cumulated activity (μCi h or MBq s); n_i = number of particles with energy E_i emitted per nuclear transition; E_i = energy per particle (MeV); f_i = fraction of energy absorbed in the target; m = mass of target region (g or kg) and k = proportionality constant (rad g/μCi h MeV or Gy kg/MBq s MeV).

The term "cumulated activity" ($\tilde{A}$) is given to the area under the time–activity curve for a source organ or region. As activity is the number of disintegrations

0969-8043/98/$19.00
PII: S0969-8043(98)00023-2

per unit time, integrating this over time gives the total number of disintegrations.

2.2. The MIRD system

The equation for absorbed dose in the Medical Internal Radiation Dose (MIRD) system (Loevinger *et al.*, 1988) is a deceptively simple representation of Eq. (1):

$$D = \tilde{A}S$$

The cumulated activity is defined above, while all other terms are lumped in the factor S:

$$S = \frac{k\sum_i n_i E_i \phi_i}{m}$$

In the MIRD equation, the factor k traditionally applied is 2.13, which gives absorbed dose in rad, from activity in μCi, mass in g and energy in MeV. With more applications currently employing the SI unit system, a factor relating absorbed dose in Gy from activity in Bq and energy in MeV may be derived and employed.

In any real internal dose problem, there will be more than one organ which concentrates the activity, and many targets for which the absorbed dose is required. In this case, the MIRD equation needs to be solved for each source region (r_h) and target region (r_k) as follows:

$$D_{r_k} = \sum_h \tilde{A}_h S(r_k \longleftarrow r_h)$$

If the area under the time–activity curve for a source organ (cumulated activity) is normalized to the amount of activity administered (A_0), this is defined as "residence time" (Loevinger *et al.*, 1988).

$$\tau_h = \frac{\tilde{A}_h}{A_0}$$

Using this definition the dose equation may be written as:

Table 1
Dose estimates given by the MIRDOSE software for In-111 white blood cells in adults and children

Target organ	Estimated radiation dose (mGy/MBq)					
	adult	15-yr-old	10-yr-old	5-yr-old	1-yr-old	newborn
Adrenals	3.6E−01	4.4E−01	6.4E−01	8.6E−01	1.4E + 00	2.9E + 00
Brain	5.1E−02	6.7E−02	8.9E−02	1.4E−01	3.0E−01	7.0E−01
Breasts	6.7E−02	7.8E−02	1.3E−01	2.0E−01	3.4E−01	7.9E−01
Gallbladder wall	3.4E−01	3.8E−01	5.8E−01	8.8E−01	1.4E + 00	3.0E + 00
LLI wall	1.2E−01	1.6E−01	2.3E−01	3.1E−01	4.7E−01	9.2E−01
Small intestine	1.6E−01	1.9E−01	2.9E−01	4.2E−01	6.7E−01	1.4E + 00
Stomach	2.9E−01	3.4E−01	5.0E−01	7.0E−01	1.1E + 00	2.3E + 00
ULI wall	1.6E−01	2.0E−01	3.1E−01	4.8E−01	7.8E−01	1.6E + 00
Heart wall	1.7E−01	2.0E−01	2.9E−01	4.1E−01	7.0E−01	1.4E + 00
Kidneys	3.5E−01	4.2E−01	6.3E−01	9.1E−01	1.4E + 00	2.7E + 00
Liver	9.0E−01	1.2E + 00	1.7E + 00	2.3E + 00	4.1E + 00	8.7E + 00
Lungs	1.6E−01	2.0E−01	2.9E−01	4.3E−01	7.4E−01	1.5E + 00
Muscle	1.0E−01	1.3E−01	1.9E−01	2.8E−01	4.9E−01	1.0E + 00
Ovaries	1.3E−01	1.6E−01	2.3E−01	3.3E−01	4.9E−01	9.9E−01
Pancreas	5.5E−01	6.5E−01	9.5E−01	1.4E + 00	2.2E + 00	4.3E + 00
Red marrow	6.5E−01	7.3E−01	1.1E + 00	2.0E + 00	4.7E + 00	1.5E + 01
Bone surfaces	4.6E−01	5.2E−01	8.3E−01	1.4E + 00	2.3E + 00	4.8E + 00
Skin	5.0E−02	6.1E−02	9.7E−02	1.6E−01	3.0E−01	6.9E−01
Spleen	5.9E + 00	8.2E + 00	1.2E + 01	1.9E + 01	3.2E + 01	8.1E + 01
Testes	3.0E−02	4.2E−02	6.7E−02	1.0E−01	1.8E−01	4.3E−01
Thymus	7.9E−02	9.3E−02	1.3E−01	1.8E−01	3.1E−01	6.6E−01
Thyroid	5.4E−02	6.7E−02	9.2E−02	1.4E−01	2.5E−01	5.6E−01
Urinary bladder wall	6.4E−02	7.8E−02	1.4E−01	1.9E−01	3.3E−01	6.0E−01
Uterus	1.0E−01	1.3E−01	1.9E−01	2.6E−01	4.1E−01	8.9E−01
Total body	1.6E−01	2.0E−01	3.1E−01	4.6E−01	8.2E−01	1.8E + 00
Effective dose equivalent	6.4E−01	8.4E−01	1.2E + 00	1.9E + 00	3.4E + 00	8.5E + 00
Effective dose (mSv/MBq)	4.1E−01	5.2E−01	7.7E−01	1.2E + 00	2.2E + 00	5.6E + 00

Assumed residence times: liver, 2.45E + 01 h; red marrow, 3.92E + 01 h; spleen, 2.45E + 01 h and remainder of the body, 9.80E + 00 h.

$$D_{r_k} = A_0 \sum_h \tau_h S(r_k \longleftarrow r_h)$$

Values of cumulated activity ($\tilde{A}$) or residence time (τ) must be developed for those organs where the activity concentrates (e.g. liver, kidneys, spleen, thyroid), the organs involved in excretion of the compound from the body (e.g. urinary bladder, intestines) and the remainder of the body. Then, the absorbed dose is calculated by multiplying the values of $\tilde{A}$ (or τ) by the appropriate S values. The software package MIRDOSE (Stabin, 1996) has facilitated this process. The software will provide the user with S tables for 10 different model individuals and will also calculate absorbed dose estimates, if the user tells the program the appropriate values of τ. A sample of the information which can be easily obtained from the software is shown in Table 1. Here, residence times for In-111 white blood cells (Stabin, 1995) are used with all of the phantoms for adults and children to obtain dose estimates to organs, as well as the effective dose equivalent and effective dose (discussed below).

Another program, MABDOSE (Johnson, 1988) has been proposed as well, which also performs dose calculations, with the possible inclusion of tumor source regions, and integration of organ time–activity curves (the MIRDOSE software requires that the user perform these integrations separately).

3. Applications

3.1. The MIRD pamphlets, DE reports

The (MIRD) Committee of the Society of Nuclear Medicine (SNM) has published many useful reports and other aids to calculating absorbed dose estimates in nuclear medicine applications. First, there is a series of technical reports, called MIRD Pamphlets, which contain much useful information. A partial listing is provided in Table 2. Some of the pamphlets, for instance those which included old compilations of decay data, were omitted. Of the ones that are listed, many remain quite useful, as they contain information which is available nowhere else and which is useful in many practical problems today (e.g. the pamphlets giving photon absorbed fractions for small objects). There is also a series of reports that detail metabolic models and dose estimates for various radiopharmaceuticals. These are called dose estimate reports (DERs) and are listed in Table 3. A number of the dose estimate reports pertain to radiopharmaceuticals not in current use, but many, particularly the ones for sodium iodide and sodium pertechnetate, continue to have useful application. The more current reports have immediate relevancy.

Table 2
Selected MIRD pamphlets

Pamphlet	Publication date	Main information	Comments
1, 1, revised	1968, 1976	discussion of MIRD internal dose technique	superceded by the MIRD primer (1988)
3	1968	photon absorbed fractions for small objects	
5, 5, revised	1969, 1978	description of anthropomorphic phantom representing reference man, photon absorbed fractions for many organs	superceded by availability of Cristy and Eckerman (1987) phantom series
7	1971	dose distribution around point sources, electron, beta emitters	
8	1971	photon absorbed fractions for small objects	same as pamphlet 3, smaller objects
11	1975	S-values for many nuclides	
12	1977	discussion of kinetic models for internal dosimetry	
13	1981	description of model of the heart, photon absorbed fractions	
14	1992	dynamic urinary bladder for absorbed dose calculations	
15	1996	description of model for the brain, photon absorbed fractions	

Table 3
MIRD dose estimate reports

Dose estimate report number	Publication reference	Compound or pharmaceutical studied
1	J. Nucl. Med. 14, 49–50, 1973	Se-75-L-selenomethionine
2	J. Nucl. Med. 14, 755–756, 1973	Ga-66-, Ga-67-, Ga-68- and Ga-72-citrate
3	J. Nucl. Med. 16, 108A–108B, 1975	Tc-99m-sulfur colloid in various liver conditions
4	J. Nucl. Med. 16, 173–174, 1975	Au-198-colloidal gold in various liver conditions
5	J. Nucl. Med. 16, 857–860, 1975	I-123, I-124, I-125, I-126, I-130, I-131 and I-132 as sodium iodide
6	J. Nucl. Med. 16, 1095–1098, 1975	Hg-197- and Hg-203-labeled chlormerodrin
7	J. Nucl. Med. 16, 1214–1217, 1975	I-123, I-124, I-126, I-130 and I-131 as sodium rose bengal
8	J. Nucl. Med. 17, 74–77, 1976	Tc-99m as sodium pertechnetate
9	J. Nucl. Med. 21, 459–465, 1980	radioxenons in lung imaging
10	J. Nucl. Med. 23, 915–917, 1982	albumin microspheres labeled with Tc-99m
11	J. Nucl. Med. 24, 339–348, 1983	Fe-52, Fe-55 and Fe-59 used to study ferrokinetics
12	J. Nucl. Med. 25, 503–505, 1984	Tc-99m diethylenetriaminepentaacetic acid
13	J. Nucl. Med. 30, 1117–1122, 1989	Tc-99m labeled bone imaging agents
14	J. Nucl. Med. 31, 378–380, 1990	Tc-99m labeled red blood cells
15	J. Nucl. Med. 33, 777–780, 1992	radioindium-lableled autologous platelets
16	J. Nucl. Med. 33, 1717–1719, 1992	Tc-99m diethylenetriaminepentaacetic acid aerosol
17	J. Nucl. Med. 34, 1382–1384, 1993	inhaled Kr-81m gas in lung imaging

3.2. Phantoms

Absorbed doses are calculated with the aid of anthropomorphic phantoms, i.e. mathematical representations of the human body, which provide the absorbed fractions and organ masses (see Eq. (1)). The first complete descriptions of a phantom representing the reference adult were given in MIRD pamphlets 5 and 5 revised (Snyder *et al.*, 1969, 1978). These absorbed fractions were used to develop the S values in MIRD pamphlet No. 11 (Snyder *et al.*, 1975). An improved set of absorbed fractions for a slightly different adult phantom and for five other individuals representing children of different ages (newborns, 1-yr-olds, 5-yr-olds, 10-yr-olds, 15-yr-olds) was published by Cristy and Eckerman (1987). Then, in 1995, four phantoms representing the adult female, both nonpregnant and at 3 stages of pregnancy were published by Stabin *et al.* (1995). Before 1995, the Cristy and Eckerman 15-yr-old phantom was often used to represent the adult female. The Stabin *et al.* adult female phantom is somewhat different than the Cristy/Eckerman model (see Table 4 and 5). The absorbed fractions for these 10 phantoms (six pediatric phantoms of Cristy and Eckerman and 4 adult female phantoms of Stabin *et al.*) are available within the MIRDOSE software. Others have as well proposed more detailed models of some organs, including the brain (Eckerman *et al.*, 1981; Bouchet, 1997), eye (Holman *et al.*, 1983), peritoneal cavity (Watson *et al.*, 1989), prostate gland (Stabin, 1994) and others.

Phantoms based on CT or MRI scans of real individuals (represented by large numbers of voxel elements) may someday replace these so-called "stylized" phantoms, but these ideas are currently under development (see Current Trends: Patient-specific dosimentry, below). Zubal *et al.* (1994) have proposed a 3-dimensional representation of an adult human for such applications. A voxel-based brain model (Tagesson *et al.*, 1996b) has also been proposed.

3.3. The proper design of kinetic studies

A valid internal dose estimate depends heavily on the collection of kinetic data for organs which concentrate the radiopharmaceutical (source organs), the whole body and for all excretion pathways. Obtaining these data require the proper measurement methods and acquisition of data at appropriate time points. The MIRD Committee has published a document which addresses these considerations (Siegel *et al.*, 1998). The document outlines the proper techniques for data quantitation and for appropriate temporal sampling. Basically, they show how to use the conjugate view technique to acquire quantitative data for dosimetry analyses, including proper choice of source and background regions, with corrections for overlapping source regions, background and scatter. The use of SPECT and PET techniques also are discussed. Quantitative methods for analyzing blood and excreta samples are described. On the subject of temporal sampling, they demonstrate that 2 or 3 time points per phase (either uptake or clearance) are needed to adequately describe the kinetics. They also show graphically the amount of error in $\tilde{A}$ (or τ) that occurs from

Table 4
Masses of source regions in the Cristy and Eckerman phantom series

Mass (g) of organ in each phantom						
	Phantom [Total Phantom Weight (kg)]					
	Newborn 3.4	age 1 9.8	age 5 19	age 10 32	15-AF 55–58	Adult Male 70
Adrenals	5.83	3.52	5.27	7.22	10.5	16.3
Brain	352	884	1260	1360	1410	1420
Breasts-including skin	0.205	1.10	2.17	3.65	407	403
Breasts-excluding skin	0.107	0.732	1.51	2.60	361	351
Gall bladder contents	2.12	4.81	19.7	38.5	49.0	55.7
Gall bladder wall	0.408	0.910	3.73	7.28	9.27	10.5
GI tract						
LLI contents	6.98	18.3	36.6	61.7	109	143
LLI wall	7.98	20.6	41.4	70.0	127	167
SI contents and wall	52.9	138	275	465	838	1100
stomach contents	10.6	36.2	75.1	133	195	260
stomach wall	6.41	21.8	49.1	85.1	118	158
ULI contents	11.2	28.7	57.9	97.5	176	232
ULI wall	10.5	27.8	55.2	93.4	168	220
Heart contents	36.5	72.7	134	219	347	454
Heart wall	25.4	50.6	92.8	151	241	316
Kidneys	22.9	62.9	116	173	248	299
Liver	121	292	584	887	1400	1910
Lungs	50.6	143	290	453	651	1000
Ovaries	0.328	0.714	1.73	3.13	10.5	8.71
Pancreas	2.80	10.3	23.6	30.0	64.9	94.3
Remaining tissue	2360	6400	13300	23100	40000	51800
Skeleton						
Active marrow	47	150	320	610	1050	1120
Cortical bone	0	299	875	1580	3220	4000
Trabecular bone	140	200	219	396	806	1000
Skin	118	271	538	888	2150	3010
Spleen	9.11	25.5	48.3	77.4	123	183
Testes	0.843	1.21	1.63	1.89	15.5	39.1
Thymus	11.3	22.9	29.6	31.4	28.4	20.9
Thyroid	1.29	1.78	3.45	7.93	12.4	20.7
Urinary bladder contents	12.4	32.9	64.7	103	160	211
Urinary bladder wall	2.88	7.70	14.5	23.2	35.9	47.6
Uterus	3.85	1.45	2.70	4.16	79.0	79.0
Whole body	3600	9720	19800	33200	56800	73700

neglecting an organ's wash-in phase or not adequately assessing the wash-out phase. The authors provide several valuable examples for many categories of calculation, which makes the document useful to the practitioner. This publication provides a useful aid in designing kinetic studies; however in each individual case it is the responsibility of the investigator to adequately describe the time–activity curves in all source organs which have a significant uptake of the radiopharmaceutical, the organs involved in the excretion of the compound and tissues in the remainder of the body.

3.4. The use of EDE and ED

Upon successfully completing a dosimetry study, the result will be a set of organ absorbed dose estimates, expressed as total absorbed dose, based on an assumed amount of administered activity or absorbed dose per unit activity administered, as shown in the section on the MIRD System, above. Also available from this information will be the estimated effective dose equivalent (EDE) (ICRP, 1979) and effective dose (ED) (ICRP, 1991). These parameters are also automatically supplied by the MIRDOSE software (Stabin *et al.*,

Table 5
Masses of source regions in the pregnant female phantom series

Mass (g) of organ in each phantom				
	Phantom			
	Adult Female (nonpregnant)	Three-month Pregnant Female	Six-month Pregnant Female	Nine-month Pregnant Female
Adrenals	14	14	14	14
Brain	1200	1200	1200	1200
Breasts-excluding skin	360	360	360	360
Gall bladder contents	50	50	50	50
Gall bladder wall	8	8	8	8
GI tract				
Lower large intestine contents	135	135	135	135
Lower large intestine wall	160	160	160	160
Small intestine contents	375	375	375	375
Small intestine wall	600	600	600	600
Stomach contents	230	230	230	230
Stomach wall	140	140	140	140
Upper large intestine contents	210	210	210	210
Upper large intestine wall	200	200	200	200
Heart contents	410	410	410	410
Heart wall	240	240	240	240
Kidneys	275	275	275	275
Liver	1400	1400	1400	1400
Lungs	651	651	651	651
Ovaries	11	11	11	11
Pancreas	85	85	85	85
Remaining tissue*	40000	39300	41700	39500
Skeleton				
Active marrow	1300	1300	1300	1300
Cortical bone	3000	3000	3000	3000
Trabecular bone	750	750	750	750
Skin	1790	1790	1790	1790
Spleen	150	150	150	150
Thymus	20	20	20	20
Thyroid	17	17	17	17
Urinary bladder contents	160	128	107	42.3
Urinary bladder wall	35.9	36.9	34.5	23.9
Uterine wall	80	374	834	1095
Fetus	–	458	1640	2960
Placenta	–	–	310	466
Whole body	58000	58000	61500	63700
Whole body (maternal tissues)	56800	56400	57500	56600

*"Remaining tissue" is defined as the part of the phantom remaining when all defined organs have been removed. This region of the phantom has been used in the radiation transport code to model muscle for dosimetric purposes. However, the appropriate mass of muscle to use in such calculations in the adult female is 15,500 g. The entries for this region have been rounded to 2 significant figures.

1996). The individual organ absorbed dose estimates are the key information that should be evaluated, especially in radionuclide therapy. The EDE and ED have no meaning when absorbed dose in the therapy realm is encountered. They are useful in the diagnostic realm, in comparing studies from different agents or from the same agent with different radionuclide labels, or in evaluating the population risk from certain studies. However, it must be remembered that these values are theoretical, being based on committee-assigned risk weighting factors for different organs and different radiobiological endpoints. These weighting factors are subject to change, as noted in the change between the EDE of ICRP 30 and the ED of ICRP 60.

The MIRD Committee has cautioned against the inappropriate use of these quantities in nuclear medicine (Poston, 1993); however, the ICRP has approved their use (ICRP, 1987, 1988) and the general consensus of the user community seems to be that these quantities have a place in risk evaluation in the diagnostic regime. For internal emitters, their use seems far more favorable than the use of the "whole body" dose (the average energy absorbed in the total body averaged over the mass of the total body), due to the nonuniform nature of radiopharmaceutical uptake and clearance which are usually encountered. Their appropriate use continues, however, to be a matter for study and debate.

3.5. Uses of absorbed dose information

The information obtained in a dosimetry study is used in many different ways, including evaluation of individual trials, and in the approval of radioactive drugs for general use. Radiation dose estimates for individual organs, usually for the two or three organs receiving the highest dose, and the EDE or ED, in the case of diagnostic studies, are used to evaluate the radiation dose expected to be received, and thus the maximum amount of activity that should be administered. Obviously in therapeutic situations, the evaluation is more important, as the radiation dose received is much higher. There are several areas of active investigation in which improvements in this information are being considered. The first, as discussed next, is the modification of current techniques to provide radiation dose estimates that are more specific to the subject under consideration, as opposed to the representation of all patients by the standardized subjects discussed in the section on Phantoms, above. Another problem that many researchers are investigating is that reported radiation dose to the red marrow often does not correlate well with observed deterministic radiation effects observed in therapy patients. This is most likely due to differences between the individual and the standard phantoms employed, not only in size and shape, but also in the health and distribution of the marrow. Most individuals involved in therapeutic trials have some form of disease which may affect marrow distribution, but as well may have received various forms of therapy previously (e.g. chemotherapy, localized external radiotherapy). Thus their red marrow may have been affected significantly, causing it to be considerably different than that in the standard model, both with regard to distribution and viability. A third area of concern currently is the calculation and interpretation of radiation dose to tissues or small structures not traditionally recognized as "organs". It is possible with current methods to calculate absorbed dose to structures of almost any size or shape (see section on Current Trends: Absorbed dose calculation, below). Selective uptake of radiopharmaceuticals and the resulting radiation dose, have been studied in the lachrymal gland (Soundy *et al.*, 1990), salivary glands (Johansson, 1997) and in small structures within the brain (Bouchet and Bolch, 1997) and the eye (Holman *et al.*, 1983). In addition, organs which have been traditionally treated as uniform in composition may in fact have regions within themselves that require separate evaluation in terms of radiation dose, such as the cortex and medulla of the kidneys (Patel, 1988). Even though it is possible to calculate this dose with good accuracy, the interpretation of this information from a safety or regulatory standpoint is not well established.

The best available information on the radiation dose from a procedure must then be used in these contexts to make decisions about the utilization of these radiopharmaceuticals. One of the areas where the information is often needed is when the subject is pregnant or potentially pregnant. The embryo or fetus is known to be radiosensitive, hence absorbed dose is often of high concern. With the release of the pregnant female phantom series (Stabin *et al.*, 1995) and incorporation of the associated absorbed fractions in the MIRDOSE software (Stabin, 1996), the calculation of absorbed dose to the embryo or fetus, at any stage of pregnancy has been greatly facilitated. However, reliable biokinetic data on which to base organ cumulated activities for the pregnant woman and the fetus itself are for the most part lacking. Russell *et al.* (1997) published absorbed dose estimates for the pregnant woman at all stages of pregnancy for many radiopharmaceuticals, but noted that the information regarding placental crossover was limited in many cases. This publication represents the best current knowledge in this area, but much more information is needed to improve these dose estimates. Another area which needs further development is the establishment of dose to individual fetal organs. The tables of Russell *et al.* give only average absorbed dose to the whole fetus. Some efforts have been made in studying absorbed dose to individual fetal organs, particularly to the fetal thyroid from iodine exposures (Watson, 1992) and some other organs (Stabin *et al.*, 1997), but this area needs substantial development. The establishment of reliable radiopharmaceutical biokinetics in the fetus is always difficult.

Information should also be shared with the subject actually undergoing the study as well, from the standpoint of providing informed consent, which is a regulatory requirement in many settings. In addition, this will assist the subject, his or her family members and others, in understanding the procedures involved and their potential risks, as well as helping them to manage their concerns associated with these areas.

The information is also useful in evaluating population dose from nuclear medicine procedures. Several authors have attempted to provide such characterizations (e.g. Cloutier *et al.*, 1984). Such analyses require reasonably accurate estimates of the numbers of nuclear medicine procedures that are performed on different subjects and the amounts of activity employed. This information is often very difficult to obtain; hence more efforts are encouraged in reporting of this type of information to facilitate better evaluations of population dose in the future.

4. Current trends

4.1. Patient-specific dosimetry

4.1.1. Motivation for patient-specific dosimetry

Radionuclide therapy based on patient-specific dosimetry offers the potential for optimizing the dose delivered to the target tumor through utilization of measured radiopharmaceutical kinetics specific to the individual. The administered activity may be tailored for the patient such that the highest possible radiation dose may be given to the tumor while limiting the dose to critical organs and tissues below any designated threshold for negative biological effects. A pretreatment quantitative dosimetry work-up using diagnostic ("tracer") activities of the therapy radiopharmaceutical serves also to identify those cancer patients for whom the treatment is likely to be most effective while eliminating those for whom it would be unsuccessful. In the case of radioimmunotherapy, these considerations are of particular importance in that the low uptake in tumor regions (low target to non-target uptake ratios) may constrain the treatment protocol (Erdi *et al.*, 1996). In addition, the use of standardized methodology for acquiring patient specific pharmacokinetic data and performing the dose calculations will increase the probability of determining the correct correlation between the estimated radiation dose and the clinically observed effects.

Ideally, the goals for treatment planning procedures using patient-specific dosimetry (DeNardo *et al.*, 1985; Strand *et al.*, 1993; Erdi *et al.*, 1996) are (Fig. 1):

(a) Acquire time sequenced quantitative data using diagnostic activities of the therapeutic radiopharmaceutical (or a suitable analogue) to determine the biodistribution over the relevant time-course for that agent. This may be achieved through sequential imaging using a planar gamma camera or tomographic systems such as single photon emission computed tomography (SPECT) or position emission tomography (PET).

(b) Estimate the radiation dose to the tumor and other target organs (critical tissues) per unit administered activity using these patient-specific biokinetic data within the MIRD calculational schema described previously. SPECT and PET have the potential for providing 3-dimensional data sets which might be used directly with Monte Carlo and other analytical algorithms to produce 3D absorbed dose maps. In these situations, it is helpful to employ X-ray computed tomography (XCT) or magnetic resonance imaging (MRI) to provide attenuation correction methods for the radionuclide scans and the anatomical base for the 3D absorbed dose maps.

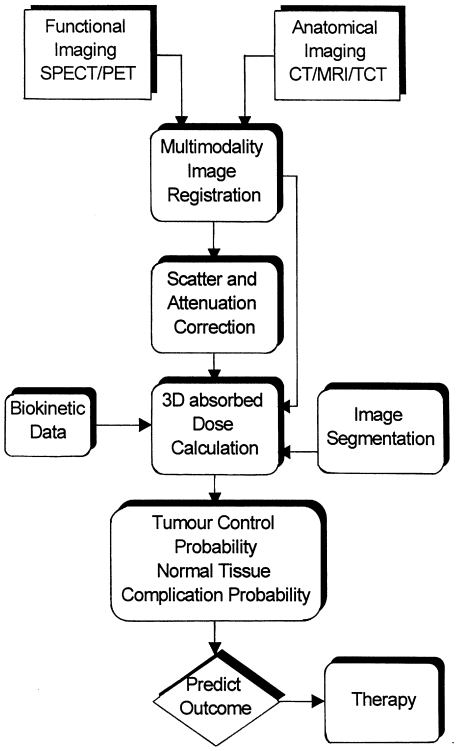

Fig. 1. Flow-chart describing the basic steps in a patient-specific dosimetry protocol.

(c) Predict the radiation dose to be delivered to the patient under the therapy regimen through extrapolation of the diagnostic dose results scaled according to the administered activities. However, it must also be recognized that biokinetics for the diagnostic and therapy administered activities might not be identical (Fielding *et al.*, 1991) as might occur if the diagnostic activity is sufficient to induce the so-call "stunning" effect on the target tissue thereby decreasing subsequent uptake. This effect has been observed in the case of diagnostic work-ups for thyroid cancer when using higher diagnostic activities.

(d) Monitor the radiopharmaceutical biokinetics during therapy for comparison with the diagnostic pre-

dictions. This satisfies the academic interest involving questions concerning the correlation of the diagnostic and therapy kinetics and allows verification of the actual therapeutic dose delivered.

(e) Evaluate the effectiveness of the therapy following treatment to predict and even avoid future possible complications in other patients. For this, dose-volume histograms (a description of the distribution of absorbed dose in histogram format), tumor control probability (TCP) and normal tissue complications probability (NTCP) should be taken into consideration (Kolbert *et al*., 1994; Niemierko and Goitein, 1994).

4.1.2. Activity quantitation

4.1.2.1. Planar techniques. A common method for *in vivo* quantitation of the activity distribution is the conjugate view approach. This method involves scintillation camera imaging that utilizes 180° opposed planar images in combination with transmission data of the subject and a system sensitivity factor (cps/MBq) that has been obtained from measurement in air (Sorenson, 1971; Thomas *et al*., 1976; Siegel *et al*., 1998). Typically, anterior and posterior (A/P) whole-body images are acquired simultaneously using a dual head scanning camera and the conjugate pair of images is calculated from the geometric mean, such that the results for source organ activity are independent of depth. Correction for photon attenuation is made by applying a transmission factor image, obtained from a measurement with an external source mounted on the other side of the patient. Scatter correction can be made by using a predefined effective attenuation coefficient or using multiple energy window methods (Ogawa *et al*., 1991). With planar imaging, the activity distribution in the patient is projected onto a 2-dimensional plane. The activity calculation is therefore limited by overlying and underlying activity distributions. Analytical and empirical methods have been developed to correct the activity quantitation for these conditions and to compensate also for the effects of scattered radiation (Siegel *et al*., 1998). Since the A/P method is a 2D method, the volume of the activity uptake is difficult to estimate. For absorbed dose calculation, the mass of the organ therefore has to be taken from a complementary imaging modality, such as CT. Since the absorbed dose is defined as the imparted energy per unit mass, this mass estimate may not be an appropriate mass to use in the absorbed dose calculation in the situation of inhomogeneous activity distribution.

4.1.2.2. Tomographic techniques: SPECT. With single-photon emission computed tomography (SPECT), a true 3D count distribution (within the camera spatial resolution limitation) representing the true activity distribution can be reconstructed from measured 2D projections around the patient. An accurate activity distribution may be obtained if proper correction for photon attenuation, scatter and collimator response is applied. Until now, a common approach has been based on a filtered backprojection reconstruction method in combination with a post-processing attenuation correction method (Chang, 1978) for photon attenuation and a dual-energy window scatter correction technique (Jaszczak *et al*., 1984). However, in modern camera systems, iterative reconstruction methods have the potential of including photon attenuation, scatter and collimator resolution in the projection step. The number of iterations needed is significantly reduced by newly developed accelerated methods, such as ordered subsets (Hudson and Larkin, 1994). These methods greatly increase the ability for obtaining accurate quantitative SPECT images. Furthermore, many vendors now include simultaneous transmission/emission SPECT hardware that can produce accurate patient outlines and attenuation maps on a routine basis.

The activity per voxel is determined from quantitative count rate SPECT images through application of the system sensitivity (cps/MBq) measured in air (Narita *et al*., 1996). A major limitation of SPECT for patient-specific absorbed dose calculations is the system spatial resolution (up to 10–20 mm FWHM), which affects the direct volume measurement of tumors and organs with dimension smaller than or comparable to this limit. PET may be an alternative, with the spatial resolution typically under 10 mm. However, the relatively expensive scanners needed and the short physical half-life of most positron-emitting radionuclides may restrict the use of PET in radionuclide treatment planning.

4.1.3. Image fusion, mass and volume determination

The information from the patient-specific attenuation distribution is important for proper attenuation correction of the SPECT data, the dose calculations and morphological-functional image fusion. With SPECT systems, simultaneous transmission-emission studies can be made with exact registration, but the spatial resolution characteristic of SPECT allows visualization only of major features such as organ outlines and lung regions. In many patient situations, a conventional CT study is routinely made prior to radionuclide therapy. Effective image registration techniques can be applied to take advantage of these anatomical images for the attenuation correction and for the 3D absorbed dose calculation. Potential problems include the fact that the CT data are obtained from X-ray spectra, thus the transformation of pixel values to attenuation coefficients and density values may not be straightforward. Furthermore, the registration of SPECT/CT images is more complex in the abdomen, where trans-

lational and rotational effects may occur. Landmarks here are difficult to define, as compared to the head, where internal structures are better defined. Successful methods have been developed, based on acquisition of Compton scatter data, for use in correlating CT images with SPECT (Sjögreen *et al.*, 1997). Image registration is also important when applying a single transmission study to sequential planar (A/P) whole-body measurements.

Accurate volume segmentation is important when determining the average absorbed dose or the distribution of absorbed doses per voxel. Different methods have been developed, including the use of grey-level thresholds (Mortelmans *et al.*, 1986) and analytical derivative techniques (King *et al.*, 1991).

4.1.4. Absorbed dose calculation

4.1.4.1. MIRD S values. For homogeneous activity distribution in organs, MIRD *S* values (Loevinger *et al.*, 1988) have been used in both diagnostic and therapy absorbed dose calculations. Program packages (Johnson, 1988; Stabin, 1996) have been proposed; as noted above in the first case, the inclusion of tumors is possible. The largest single source of error in the procedure is often in the biokinetics, especially the uncertainty in the late activity–time data. However, in situations in which the mass of the target region is difficult to determine, this may introduce the largest source of error. The use of *S* values based on standardized individuals, even if scaled using the true organ mass from patient-specific data, may also introduce significant errors into the analysis (Kolbert *et al.*, 1997). If the activity distribution is relatively uniform within the organ, the standard approximations may be relatively good, but if there are important inhomogeneities (the presence of a hot or cold tumor, etc.), calculations based on the assumption of a uniform activity distribution may be significantly in error.

4.1.4.2. Dose point kernels. For an inhomogeneous activity distribution in a homogeneous material (regarding both elemental composition and density), a dose point kernel may be used (Berger, 1973; Prestwich *et al.*, 1989; Simpkin and Mackie, 1990; Leichner, 1994). Treatment planning systems, based on dose point kernels, have been reported by several authors (Sgouros, 1993; Giap *et al.*, 1994; Akabani *et al.*, 1997). The conversion of activity to absorbed dose can be regarded as a filtering method, either as a convolution process in the spatial domain or as a multiplication in the frequency domain. When applied in the spatial domain, rescaling of the kernel distribution can be done when crossing a boundary. Applying the kernel in the frequency domain is often implemented to speed up the calculations.

4.1.4.3. Monte Carlo simulation. The major limitation with dose kernels is that they can only describe the distribution in a uniform infinite medium. This affects the accuracy in the calculation of the dose distribution at interfaces between different attenuating media (such as between lung tissue and muscle tissue). The most accurate method is therefore to fully model the interaction of photons and electrons from a patient-specific activity distribution and attenuation map using a Monte Carlo transport method (Berger, 1963; Raeside, 1976; Andreo, 1991).

In a treatment planning system, based on quantitative SPECT and Monte Carlo, the emission of photons and electrons are simulated and their paths are followed, using probability functions to govern their loss of energy, deflection/scattering angles and other events, as they pass through the system. Performing transport of all emitted particles and their secondary particles can account for inhomogeneities, both in activity, elemental composition, and density.

Public domain Monte Carlo packages, such as EGS4 (Simpkin and Mackie, 1990), MCNP and ITS (Briesmeister, 1993), are available and may be implemented in radionuclide treatment planning. More dedicated treatment planning programs, based on Monte Carlo simulations, have been reported (Furhang *et al.*, 1996, 1997; Tagesson *et al.*, 1996a). Such systems use quantitative planar- or SPECT images to establish the biokinetics of the radiopharmaceutical and the activity distribution. Information about the size, shape and mass of the organs may be obtained from these data by, for example, segmentation methods. The information derived from these sequential images provides the activity as a function of time, which can, as discussed above, be used to calculate the absorbed dose rate as a function of time and location within the subject. The dose rate is then integrated to obtain the cumulative dose to individual organs, regions, etc. These data may be analyzed as an absorbed dose distribution, in terms of total absorbed dose to different regions, dose-volume histograms, etc., with the hope that such information will provide a more comprehensive evaluation of the therapy effect.

4.1.5. Complementary measurements

Blood sampling, urine and feces collection provide additional information on the activity distribution. In radionuclide therapy, especially radioimmunotherapy, besides knowing the activity content in tumors and tissues, the absorbed dose distribution is needed for proper evaluation of the therapeutic efficacy. For such measurements film autoradiography may be used. Although it is slow, it has a very good resolution (from 10–100 mm). Film may also be replaced by the much faster fluorescent plates, which have resolutions between 50–150 mm. This method has the disadvan-

tage of an inability to obtain real time images, thus preventing direct user controlled sampling. Also, only one radionuclide can be imaged simultaneously due to the lack of energy resolution. Solid state detectors, such as the silicon beta camera (Overdick *et al*., 1997) are also under development. Using a high resolution detector for imaging and direct digitization, a 3D-image matrix of the activity distribution may be created, which in turn may be used to obtain a 3D-absorbed dose distribution (Ljunggren and Strand, 1990; Strand *et al*., 1991).

Autoradiography, especially electron microscopy autoradiography, can also show activity distributions within cells. Thus, radionuclide distributions may be observed at the subcellular level (Jonsson *et al*., 1992a,b). Jonsson *et al*. showed for ^{111}In that there may be a very heterogenous distribution of ^{111}In in different tissues after i.v. injection.

4.2. Small scale dosimetry and microdosimetry

4.2.1. General considerations

When the uptake of a radiopharmaceutical in a target tissue is particularly nonuniform, the averaging of the dose over the entire tissue may be an oversimplification of the actual energy deposition pattern. In order to provide appropriate information for interpretation of the dose, the detailed energy deposition pattern over short (i.e. cellular) ranges may need to be studied. This is especially important for short range radiations (e.g. low-energy photons, internal conversion electrons (ICE), Auger electrons (AE), Coster–Kronig electrons) which may be absorbed within a short distance.

The work of Rao *et al*. (1983) with mouse testes demonstrated that Tl-201, which emits predominantly low energy mercury X-rays, AEs and ICEs, was two to four times more effective in reducing testis weight and sperm number than Tl-204 (a high energy beta emitter) per unit activity administered. However, this result is contrary to what one would expect by considering only the total testicular dose per unit activity of Tl-201 and Tl-204 in the organ as calculated by conventional dosimetry. Thus it appears that the abundance of low-energy electrons emitted during Tl-201 decay, which deliver the majority of their energy over a very short range, have a more significant influence over the measured biologic effect than the average total energy deposited per gram would have predicted. On the other hand, if one were to consider In-111 platelet scintigraphy, the situation may be reversed. A 50 mGy organ dose to the spleen is predicted during radioplatelet imaging with modest amounts (10 MBq) of injected activity. It is important to remember, however, that the 50 mGy splenic dose calculation was made by dividing the energy from radiation absorbed in the spleen during decay by the organ's entire mass. This simplification ignores the fact that a significant fraction of the particulate radiation emitted by ^{111}In is in the form of low-energy (0.6–25.4 keV) Auger electrons, which undoubtedly deposit some of their energy within the platelet itself or in adjacent platelets within small platelet formations. Thus, in this case, the estimated average dose may overestimate the actual energy deposition pattern for sensitive sites within cells of the spleen. When Auger electron emitters are incorporated into tissues, especially if the subcellular distribution is close to the nucleus and the DNA, the biological effect can be high. As an example, for ^{125}I incorporated into DNA the effect is as severe as for a-particle emitters. This has elegantly been shown by Sastry and Rao (1992) for ^{125}IUdR and ^{210}Po in the cell nucleus, whereas for activity distributed in the cytoplasm the effect is not seen. A good summary of the dosimetry for Auger emitters is given in the AAPM reports (Humm *et al*., 1994) and in papers from the 3rd Symposium on Auger Processes in Lund 1995 (Third International Symposium on Biophysical Aspects of Auger Processes, 1997). The MIRD concept, with absorbed fractions and *S*-values on the cellular level, has also been employed to calculate absorbed doses at the cellular level (Goddu *et al*., 1994a,b).

4.2.2. Calculational techniques

Calculating absorbed dose as a function of distance from point or extended photon sources or from electron-emitting sources has been facilitated for many years by the formulas of Loevinger *et al*. (1956) and the point kernels of Berger (1971a). Through the use of these methods, dose as a function of distance may be estimated for most source geometries. Berger, in a related paper (Berger, 1971b), showed formulae for estimation of dose distributions from distributed sources of activity, using geometry factors in integrals involving the point source functions. More recently, similar efforts have been attempted by Howell *et al*. (1989), Werner *et al*. (1991) and Cross *et al*. (1992). As noted above, radiation transport codes are also available which can simulate the transport and absorption of photon and electron energy. These codes model the transport of electrons and photons, after the geometries of the source and target regions have been established using standard geometry approximations (planes, spheres, cylinders, etc.). The codes provide estimates of the energy deposition in the various regions and estimates of the errors associated with the calculated values. The codes provide the ability to account for many real physical processes often not addressable with point kernels (e.g. crossing boundaries of regions with different densities and composition, electron backscattering). Their use, however, necessitates a considerable amount of learning on the part of the user in order to successfully model a system

and obtains meaningful results. The point kernels of Berger and Cross *et al.* were originally generated through the use of similar codes; however these simulations assumed an infinite homogeneous medium. Useful applications of the use of point kernels have been published by a number of authors, including Howell *et al.* (1989), Werner *et al.* (1991), Hui *et al.* (1992) and Faraggi *et al.* (1994), usually for activity in and around tumors of various sizes.

4.3. Alpha emitters

With the relatively recent entry of alpha-emitting radiopharmaceuticals as candidates for therapy, several new considerations emerge. When radionuclides with only photon or electron emissions are involved in radiation dose calculations, whether to calculate absorbed dose or equivalent dose is not much of an issue, and the two are thought to be numerically identical, as all radiation weighting factors (w_R) to be assigned are 1.0 (ICRP, 1991). For alpha emitters, the assigned value of w_R for purposes of protecting workers is set at 20 (ICRP, 1991), but for the evaluation of dosimetry and safety with internal emitters, an appropriate value is not clear. One suggestion at present is to use a value of 5 (Zalutsky *et al.*, 1997), but clearly more investigation and guidance from regulatory and international advisory bodies is needed.

With alpha emitters also, however, there is often the need to evaluate not only average organ, tumor, or tissue dose, but also microdosimetric quantities, as described in ICRU Publication 36 (1983) and demonstrated by several investigators (e.g. Goddu *et al.*, 1994a,b). These microdosimetric quantities may be calculated analytically or by Monte Carlo methods (Stinchcomb and Roeske, 1992). Although the calculational methods are somewhat standardized and agreed upon, publication and distribution of tools to help in the standardized calculation of these quantities has not progressed nearly to the same level as for small scale or macrodosimetry and the investigator is usually left to develop such calculations on his or her own. Furthermore, the interpretation of the information obtained from these analyses has not been clearly elucidated. The biological significance of specific energy distributions, of the dose to small regions, and of dose distributions within regions remains to be more fully explained in order for the information coming from the dosimetric analyses discussed above to be used in a meaningful way. Nonetheless, many tools exist for the calculation of radiation dose in a variety of situations and development continues in the areas of calculational methods and biological response models.

Acknowledgements

This work have been partly funded by the Swedish Radiation Protection Institute #963.96, the Gunnar Nilsson Foundation, Sweden and the Kamprad Foundation, Sweden.

References

Akabani, G., Hawkins, W. G., Eckblade, M. B., Leichner, P. K., 1997. Patient-specific dosimetry using quantitative SPECT imaging and three-dimensional discrete fourier transform convolution. J. Nucl. Med. 38, 308–314.

Andreo, P., 1991. Review: Monte Carlo techniques in medical radiation physics. Phys. Med. Biol. 36, 861–920.

Berger, M., 1971a. MIRD Pamphlet No. 7: Distribution of absorbed dose around point sources of electrons and beta particles in water and other media. J. Nucl. Med. Suppl. 5, 5.

Berger, M., 1971b. Beta-ray dosimetry calculations with the use of point kernels. In *Proc. Medical Radionuclides: Radiation Dose and Effects*, Oak Ridge, TN, Dec. 8–11, 1969. U.S. Atomic Energy Commission.

Berger, M., 1973. Improved point kernels for electron and beta ray dosimetry. Center for Radiation Research, Department of Commerce, Washington D.C., U.S.A.

Berger, M., 1963. Monte Carlo calculation of the penetration and diffusion of fast charged particles. In *Methods in Computional Physics*, eds. S. Fernbach and M. Rotenberg, Vol. 1, pp. 135–215. Academic, New York.

Bouchet, L., 1997. Five new pediatric head and brain models for internal dosimetry calculations for photon, electron and positron sources. J. Nucl. Med. 38 (5), 105P–106P Abstract.

Briesmeister, J., 1993. MCNP: A general Monte Carlo n-particle transport code. *MCNP User's Manual*. Los Alamos National Laboratory.

Chang, L. T., 1978. A method for attenuation correction in radionuclide computed tomography. IEEE Trans. Nucl. Sci. 25, 638–643.

Cloutier, R., Watson, E., Stabin, M., 1984. Applying the ICRP risk factors to nuclear medicine doses. Proceedings of Sixth Congress of the International Radiation Protection Association Meeting, West Berlin. In *Compacts* 1, 497–500.

Cristy, M., Eckerman, K., 1987. Specific absorbed fractions of energy at various ages from internal photons sources. ORNL/TM-8381 V1-V7. Oak Ridge National Laboratory, Oak Ridge, TN.

Cross, W., Freedman, N., Wong, P., 1992. Tables of Beta-Ray Dose Distributions in Water. Chalk River Nuclear Laboratories, Chalk River, Ontario. AECL-10521.

DeNardo, G. L., Raventos, A., Hines, H. H., Scheibe, P. O., Macey, D. J., Hays, M. T., DeNardo, S. J., 1985. Requirements for a treatment planning system for radioimmunotherapy. Int. J. Radiat. Oncol. Biol. Phys. 11, 335–348.

Eckerman, K., Cristy, M., Warner, G., 1981. Dosimetric evaluation of brain scanning agents. In *Third International Radiopharmaceutical Dosimetry Symposium*, eds. E. E. Watson, A. T. Schlafke-Stelson, J. L. Coffey and R. J.

Cloutier, pp. 527–540. HHS Publication FDA 81-8166, U.S. Department of Health and Human Services, Food and Drug Administration, Rockville, MD.

Erdi, A. K., Erdi, Y. E., Yorke, E. D., Wessels, B. W., 1996. Treatment planning for radio-immunotherapy. Phys. Med. Biol. 41, 2009–2026.

Faraggi, M., Gardin, I., de Labroille-Vaylet, C., Moretti, J., Bok, B., 1994. The influence of tracer localization on the electron dose rate delivered to the cell nucleus. J. Nucl. Med. 35 (1), 113–119.

Fielding, S. L., Flower, M. A., Ackery, D., Kemshead, J. T., Lashford, L. S., Lewis, I., 1991. Dosimetry of Iodine 131 meta-iodobenzylquanidine for treatment of resistant neuroblastoma: Results of a UK study. Eur. J. Nucl. Med. 18, 308–316.

Furhang, E. E., Chui, C. S., Kolbert, K. S., Larson, S. M., Sgouros, G., 1997. Implementation of a Monte Carlo dosimetry method for patient-specific internal emitter therapy. Med. Phys. 24, 1163–1172.

Furhang, E. E., Chui, C. S., Sgouros, G., 1996. A Monte Carlo approach to patient-specific dosimetry. Med. Phys. 23, 1523–1529.

Giap, H. B., Macey, D. J., Poduloff, D. A., Boyer, A. L., 1994. Development of a SPECT-based 3D methodology for internal dosimetry of radioimmunotherapy. J. Nucl. Med. 35, 123P.

Goddu, S., Howell, R., Rao, D., 1994a. Cellular dosimetry: absorbed fractions for monoenergetic electron and alpha particle sources and *S*-values for radionuclides uniformly distributed in different cell compartments. J. Nucl. Med. 35, 303–316.

Goddu, S. M., Rao, D. V., Howell, R. W., 1994b. Multicellular dosimetry for micrometastases: Dependence of self-dose vs cross-dose to cell nuclei on type and energy of radiation and subcellular distribution of radionuclides. J. Nucl. Med. 35, 521–530.

Holman, B., Zimmerman, R., Schapiro, J., Kaplan, M., Jones, A., Hill, T., 1983. Biodistribution and dosimetry of *n*-isopropyl-*p*-[123I]iodoamphetamine in the primate. J. Nucl. Med. 24 (10), 922–931.

Howell, R., Rao, D., Sastry, K., 1989. Macroscopic dosimetry for radioimmunotherapy: Non-uniform activity distributions in solid tumors. Med. Phys. 16 (1), 66–74.

Hudson, H. M., Larkin, R. S., 1994. Accelerating image reconstruction using ordered subsets of projection data. IEEE Trans. Med. Imag. 13, 601–609.

Hui, E., Fisher, D., Press, O. et al, 1992. Localized beta dosimetry of 131I-labeled antibodies in follicular lymphoma. Med. Phys. 19 (1), 97–104.

Humm, J. L., Howell, R. W., Rao, D. V., 1994. Dosimetry of Auger-electron-emitting radionuclides: Report No. 3 of AAPM Nuclear Medicine Task Group No. 6. Med. Phys. 21, 1901–1915.

International Commission of Radiation Units and Measurements, 1983. Microdosimetry. ICRU Report 36. International Commission on Radiation Units and Measurements.

International Commission on Radiological Protection, 1979. Limits for Intakes of Radionuclides by Workers. ICRP Publication 30. Pergamon Press, New York.

International Commission on Radiological Protection, 1987. Protection of the Patient in Nuclear Medicine. ICRP Publication 52. Pergamon Press, New York.

International Commission on Radiological Protection, 1988. Radiation Dose to Patients from Radiopharmaceuticals. ICRP Publication 53. Pergamon Press, New York.

International Commission on Radiological Protection, 1991. 1990 Recommendations of the International Commission on Radiological Protection. ICRP Publication 60. Pergamon Press, New York.

Jaszczak, R. J., Greer, K. L., Floyd, C. E., Harris, C. C., Coleman, R. E., 1984. Improved SPECT quantification using compensation for scattered photons. J. Nucl. Med. 25, 893–900.

Johansson, L., 1997. Absorbed dose in salivary glands from technetium-99m labeled radiopharmaceuticals. In *Proc. Sixth International Radiopharmaceutical Dosimetry Symposium*. Oak Ridge Associated Universities (in press).

Johnson, T. K., 1988. MABDOSE: a generalized program for internal radionuclide dosimetry. Comput. Methods Programs Biomed. 27, 159–167.

Jonsson, B. A., Strand, S. E., Larsson, B. S., 1992a. A quantitative autoradiographic study of the heterogeneous activity distribution of different indium-111-labeled radiopharmaceuticals in rat tissues. J. Nucl. Med. 33, 1825–1833.

Jonsson, B.-A., Strand, S.-E. Emanuelsson, H., Larsson, B. S., 1992b. Tissue, cellular and subcellular distribution of indium radionuclides in the rat. In *Biophysical Aspects of Auger Processes*, eds. R. W. Howell, V. R. Narra, K. S. R. Sastry, D. V. Rao, AAPM Symposium Series No. 8, pp. 249–272. American Association of Physicists in Medicine (AAPM), Woodury, New York.

King, M. A., Long, D. T., Brill, A. B., 1991. SPECT volume quantitation: Influence of spatial resolution, source size and shape and voxel size. Med. Phys. 18, 1016–1024.

Kolbert, K. S., Sgouros, G., Scott, A. M., Baldwin, B., Zhang, J., Kalaigian, H., Macapinlac, H. A., Graham, M. C., Larson, S. M., 1994. Dose-volume histogram representation of patient dose distribution in 3-dimensional internal dosimetry. J. Nucl. Med. 35, 123P.

Kolbert, K. S., Sgouros, G., Scott, A. M., Bronstein, J. E., Malane, R. A., Zhang, J. J., Kalaigian, H., Mcnamara, S., Schwartz, L., Larson, S. M., 1997. Implementation and evaluation of patient-specific three-dimensional internal dosimetry. J. Nucl. Med. 38, 301–308.

Leichner, P. K., 1994. A unified approach to photon and beta particle dosimetry. J. Nucl. Med. 35, 1721–1729.

Loevinger, R., Japha, E., Brownell, G., 1956. Discrete radioisotope processes. In *Radiation Dosimetry*, eds. G. Hine and G. Brownell, Chap. 16, pp. 694–802. Academic Press, New York.

Ljunggren, K., Strand, S.-E., 1990. Beta camera for static and dynamic imaging of charged-particle emitting radionuclides in biologic samples. J. Nucl. Med. 31, 2058–2063.

Loevinger, R., Budinger, T., Watson, E., 1988. MIRD Primer for Absorbed Dose Calculations. Society of Nuclear Medicine.

Mortelmans, L., Nuyts, J., Van Pamel, G., Van den Maegdenburgh, V., De Roo, M., Suetens, P., 1986. A new thresholding method for volume determination by SPECT. Eur. J. Nucl. Med. 12, 284–290.

Narita, Y., Eberl, S., Iida, H., Hutton, B. F., Braun, M., Nakamura, T., Bautovich, G., 1996. Monte Carlo and experimental evaluation of accuracy and noise properties of two scatter correction methods for SPECT. Phys. Med. Biol. 41 (11), 2481–2496.

Niemierko, A., Goitein, M., 1994. Dose-volume distributions: A new approach to dose-volume histograms in three-dimensional treatment planning. Med. Phys. 21, 3–11.

Ogawa, K., Harata, H., Ichihara, T., Kubo, A., Hashimoto, S., 1991. A practical method for position dependent Compton-scatter correction in single photon emission CT. IEEE Trans. Med. Imag. 10, 408–412.

Overdick, M., Czermak, A., Fischer, P. et al., 1997. A Bioscope system using double-sided silicon strip detectors and self-triggering read-out chips. *Nucl. Instrum. Methods* (submitted).

Patel, J., 1988. A revised model of the kidney for medical internal radiation dose calculations. WHC-SA-0744. Westinghouse Hanford Company, Hanford, WA.

Poston, J., 1993. Application of the effective dose equivalent to nuclear medicine patients. J. Nucl. Med. 34 (4), 714–716.

Prestwich, W. V., Nunes, J., Kwok, C. S., 1989. Beta dose point kernels for radionuclides of potential use in radioimmunotherapy. J. Nucl. Med. 30, 1036–1046.

Raeside, D. E., 1976. Monte Carlo principles and applications. Phys. Med. Biol. 21, 181–197.

Rao, D. V., Govelitz, D. F., Sastry, K. S. R., 1983. Radiotoxity of thallium-201 in mouse testes: inadequacy of conventional dosimetry. *J. Nucl. Med.* **24**, 145–153.

Russell, J. R., Stabin, M. G., Sparks, R. B., Watson, E. E., 1997. Radiation absorbed dose to the embryo/fetus from radiopharmaceuticals. Health Phys. J. 73 (5), 756–769.

Sastry, K., Rao, D. V., 1992. Biological effects of the Auger emitter iodine-125: A review. Report No. 1 of AAPM Nuclear Medicine Task Group No. 6. Med. Phys. 19, 1361–1370.

Sgouros, G., 1993. Bone marrow dosimetry in radioimmunotherapy: theoretical considerations. J. Nucl. Med. 34, 689.

Sgouros, G., Chui, S., Pentlow, K. S., Brewster, L. J., Kalaigian, H., Baldwin, B., Daghighian, F., Graham, M. C., Larson, S. M., Mohan, R., 1993. 3-Dimensional dosimetry for radioimmunotherapy treatment planning. J. Nucl. Med. 34, 1595–1601.

Siegel, J., Thomas, S., Stubbs, J., Stabin, M., Hays, M., Koral, K. et al., 1998. Techniques for quantitative radiopharmaceutical biodistribution data acquisition and analysis for use in human radiation dose estimates. *MIRD Pamphlet No. 16* (in press).

Simpkin, D. J., Mackie, T. R., 1990. EGS4 Monte Carlo determination of the beta dose kernel in water. Med. Phys. 17, 179–186.

Sjögreen, K., Ljungberg, M., Erlandsson, K., Floreby, L., Strand, S., 1997. Registration of abdominal CT and SPECT images using Compton scatter data. *Proceedings of the Information Processing in Medical Imaging*.

Snyder, W., Ford, M., Warner, G., Fisher, H., Jr., 1969. MIRD Pamphlet No. 5: Estimates of absorbed fractions for monoenergetic photon sources uniformly distributed in various organs of a heterogeneous phantom. J. Nucl. Med. Suppl. 3, 5.

Snyder, W., Ford, M., Warner, G., Watson, S., 1975. "*S*", absorbed dose per unit cumulated activity for selected radionuclides and organs. *MIRD Pamphlet No. 11*. Society of Nuclear Medicine, New York, NY.

Snyder, W., Ford, M., Warner, G., 1978. Estimates of specific absorbed fractions for photon sources uniformly distributed in various organs of a heterogeneous phantom. *MIRD Pamphlet No. 5*. Society of Nuclear Medicine, New York (revised).

Sorenson, J. A., 1971. Methods for quantitating radioactivity *in vivo* by external counting measurements. Thesis, University of Wisconsin, Madison.

Soundy, R., Tyrrell, D., Pickett, R., Stabin, M., 1990. The radiation dosimetry of Tc-99m-exametazime. Nucl. Med. Commun. 11, 791–799.

Stabin, M. G., 1994. A model of the prostate gland for use in internal dosimetry. J. Nucl. Med. 35 (3), 516–520.

Stabin, M. G., 1995. Internal dosimetry in pediatric nuclear medicine. In *Pediatric Nuclear Medicine*, Chap. 26, pp. 556–581. Springer-Verlag, New York.

Stabin, M., 1996. MIRDOSE: the personal computer software for use in internal dose assessment in nuclear medicine. J. Nucl. Med. 37, 538–546.

Stabin, M., Watson, E., Cristy, M., Ryman, J., Eckerman, K., Davis, J., Marshall, D., Gehlen, K., 1995. Mathematical models and specific absorbed fractions of photon energy in the nonpregnant adult female and at the end of each trimester of pregnancy. ORNL Report ORNL/TM-12907.

Stabin, M., Stubbs, J., Toohey, R., 1996. Radiation dose estimates for radiopharmaceuticals. NUREG/CR-6345. U.S. Nuclear Regulatory Commission, Washington, D.C.

Stabin, M., Stubbs, J. B., Russell, J. R., 1997. Review of the radiation doses received by infants irradiated in-utero in Fe-59 Studies at Vanderbilt University in the 1940's. Health Phys. J. 72, 701–707.

Stinchcomb, T., Roeske, J., 1992. Analytic microdosimetry for radioimmunotherapeutic alpha emitters. Med. Phys. 19 (6), 1385–1393.

Strand, S.-E., Ljunggren, K., Kairemo, K., Svedberg, A., Norrgren, K., Ingvar, C., Wanying, Q., 1991. Functional imaging and dosimetric applications of the beta camera in radioimmunodiagnosis and radioimmunotherapy. Antib. Immunoconj. Radiopharm. 4, 631–635.

Strand, S., Hjonsson, B., Ljungberg, M., Tennvall, J., 1993. Radioimmunotherapy dosimetry: a review. Acta Oncol. 33, 807–817.

Tagesson, M., Ljungberg, M., Strand, S.-E., 1996a. A Monte Carlo program converting activity distributions to absorbed dose distributions in a radionuclide treatment planning system. Acta Oncol. 35, 367.

Tagesson, M., Zubal, I. G., Ljungberg, M., Strand, S.-E., 1996b. Absorbed fractions and *S*-values for subregions in the brain. *Proceedings of the 6th International Radiopharmaceutical Dosimetry Symposium*. Oak Ridge, TN, U.S.A.

Thomas, S. R., Maxon, H. R., Kereiakes, J. G., 1976. *In vivo* quantitation of lesion radioactivity using external counting methods. Med. Phys. 3, 253–255.

Third International Symposium on Biophysical Apsects of Auger Processes, 1997. Scandinavian University Press, pp. 783–964.

Watson, E. E., 1992. Radiation absorbed dose to the human fetal thyroid. In *Fifth International Radiopharmaceutical Dosimetry Symposium*, pp. 179–187. Oak Ridge Associated Universities, Oak Ridge, Tennessee.

Watson, E. E., Stabin, M. G., Davis, J. L., Eckerman, K. F., 1989. A model of the peritoneal cavity for use in internal dosimetry. J. Nucl. Med. 30, 2002–2011.

Werner, B., Rahman, M., Salk, W., 1991. Dose distributions in regions containing beta sources: Uniform spherical source regions in homogeneous media. Med. Phys. 18 (6), 1181–1191.

Zalutsky, M., Stabin, M., Larsen, R., Bigner, D., 1997. Tissue distribution and radiation dosimetry of astatine-211 labeled chimeric 81C6, an a-particle-emitting immunoconjugate. Nucl. Med. Biol. 24 (3), 255–261.

Zubal, I. G., Harrell, C. R., Smith, E. O., Rattner, Z., Gindi, G., Hoffer, P. B., 1994. Computerized 3-dimensional segmented human anatomy. Med. Phys. 21, 299–302.